

Dynamical entanglement purification using chains of atoms and optical cavities

Denis Gonta^{1,*} and Peter van Loock^{1,†}

¹*Optical Quantum Information Theory Group, Max Planck Institute for the Science of Light, Günther-Scharowsky-Str. 1, Building 26, 91058 Erlangen, Germany*

(Dated: June 22, 2022)

In the framework of cavity QED, we propose a practical scheme to purify dynamically a bipartite entangled state using short chains of atoms coupled to high-finesse optical cavities. In contrast to conventional entanglement purification protocols, we avoid CNOT gates, thus reducing complicated pulse sequences and superfluous qubit operations. Our interaction scheme works in a deterministic way, and together with entanglement distribution and swapping, opens a route towards efficient quantum repeaters for long-distance quantum communication.

PACS numbers: 03.67.Hk, 42.50.Pq, 03.67.Mn

I. INTRODUCTION

In classical data transmission, repeaters are used to amplify the data signals (bits) when they become weaker during their propagation. In long-distance optical-fiber systems, for instance, repeaters are used to compensate for the intensity losses caused by scattering and absorption of light pulses propagating along the fibre. In contrast to classical information, the above procedure is impossible to realize when the transmitted data signals carry bits of quantum information (qubits). In an optical-fiber system, a qubit can be encoded into a single photon which cannot be amplified or cloned without destroying quantum coherence associated with this qubit [1, 2]. Therefore, the photon has to propagate along the entire length of the fiber which causes an exponentially decreasing probability to detect this photon at the end of the channel.

To avoid the exponential decay of a photon wavepacket and preserve its quantum coherence, the concept of a quantum repeater was proposed [3]. According to this concept, a large set of entangled photon pairs is distributed over sufficiently short fiber segments. The two protocols (i) entanglement purification [4, 5] and (ii) entanglement swapping [6] are employed to extend the short-distance entangled photon pairs over the entire length of the channel. With the help of entanglement swapping, two entangled pairs of neighboring segments are combined into one entangled pair, gradually increasing the distance of shared entanglement. The entanglement purification enables one to distill high-fidelity entangled pairs from a larger set of low-fidelity entangled pairs by means of local operations performed in each of the repeater nodes and classical communication between these nodes. The resulting entangled photon pair distributed between the end points of the photonic channel can then be used for quantum teleportation [7] or quantum key distribution [8].

Owing to the fragile nature of quantum correlations and inevitable photon loss in the transmission channel, it still poses a serious challenge for experimentalists to outperform the direct transmission of photons along the fiber. Up to now, only individual building blocks of a quantum repeater have been experimentally demonstrated including bipartite entanglement purification [9, 10], entanglement swapping [11, 12], and entanglement distribution between two neighboring nodes [13, 14]. Nevertheless, motivated both by the impressive experimental progress and theoretical advances, various revised and improved implementations of repeaters or its building-blocks have been proposed [15–28].

Practical schemes for implementing a quantum repeater are not straightforward. The two mentioned protocols, entanglement purification and entanglement swapping, require feasible and reliable quantum logic, such as single- and two-qubit gates. Due to its complexity and high demand of physical resources, entanglement purification is the most delicate and cumbersome part of a quantum repeater.

In one of the purification protocols [5], two repeater nodes A and B share a finite set of low-fidelity entangled pairs grouped into elementary blocks of two qubit pairs as displayed in Fig. 1(a). Each entangled pair is given by the Werner state [29]

$$\rho_f^{AB} = f \Phi_{AB}^+ + \frac{1-f}{3} (\Phi_{AB}^- + \Psi_{AB}^+ + \Psi_{AB}^-), \quad (1)$$

being diagonal in the usual Bell basis, with $\Phi_{AB}^\pm \equiv |\phi_{AB}^\pm\rangle\langle\phi_{AB}^\pm|$, $\Psi_{AB}^\pm \equiv |\psi_{AB}^\pm\rangle\langle\psi_{AB}^\pm|$. The fidelity

$$\mathbf{F}(\rho_f^{AB}) \equiv \text{Tr} [\Phi_{AB}^+ \rho_f^{AB}] = f > 0.5 \quad (2)$$

is assumed to be above the threshold value of 1/2. Both qubit pairs (from each elementary block) are assumed to interact locally, i.e., such that the interaction occurs only within one single repeater node (A and B) as indicated by grey ellipses in Fig. 1(a). More specifically, the qubit pairs $1_A - 2_A$ and $1_B - 2_B$ are first rotated with help of single-qubit gates $U_\pm = \frac{1}{\sqrt{2}}(I \pm i\sigma_x)$, with the usual Pauli operators, and afterwards interact by means

* denis.gonta@mpl.mpg.de

† peter.vanloock@mpl.mpg.de

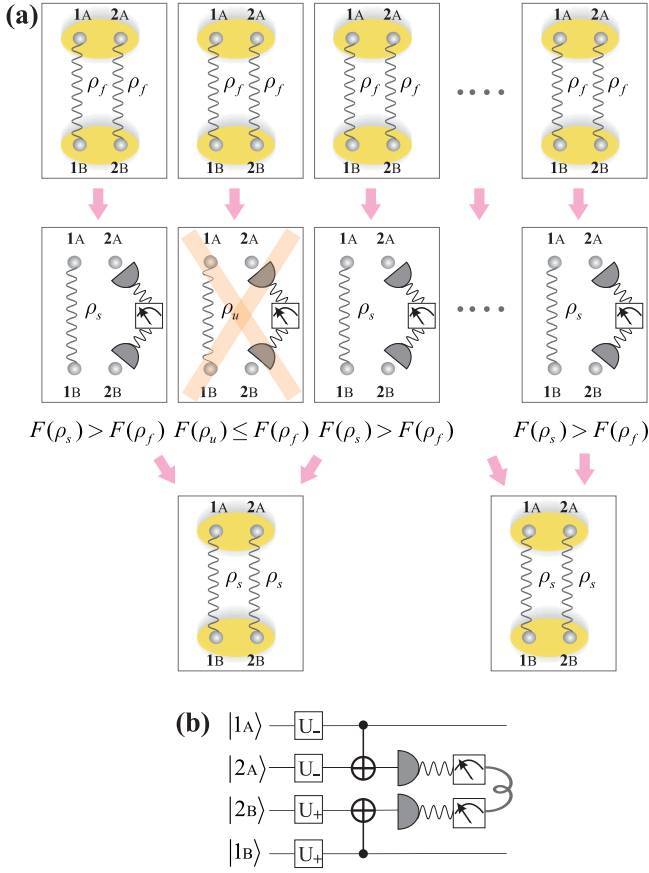


FIG. 1. (Color online) (a) Sequence of steps for the conventional purification protocol described in the text. In the upper part, repeater nodes A and B share a set of low-fidelity entangled pairs grouped into elementary blocks of four qubits, and the grey ellipses indicate local interactions occurring within each repeater node. In the middle part, one qubit pair (inside each elementary block) is projectively measured and the results are compared with a predefined outcome. In the lower part, all successfully purified qubit pairs are collected and the purification takes place one more time. (b) Quantum circuit that corresponds to the interaction indicated above by grey ellipses. See description of gates in the text.

of CNOT gates as shown in Fig. 1(b). By means of the latter gate, qubit 1_A (1_B) acts as control qubit and qubit 2_A (2_B) as target qubit. While the control qubit does not change its state under the CNOT gate, the target qubit is flipped once the control qubit is set to the excited state. In order to simplify our further discussions, the entire sequence of quantum gates indicated by grey ellipses shall be referred to below as the purification gate. After the purification gate is performed, qubits 2_A and 2_B are projected on the computational basis $\{|0\rangle, |1\rangle\}$ and the outcome of these projections is exchanged between the two nodes by means of classical communication [see the middle part of Fig. 1(a)].

Entanglement purification is successful if the outcome of projections reads $\{0, 0\}$ or $\{1, 1\}$ for qubits 2_A and

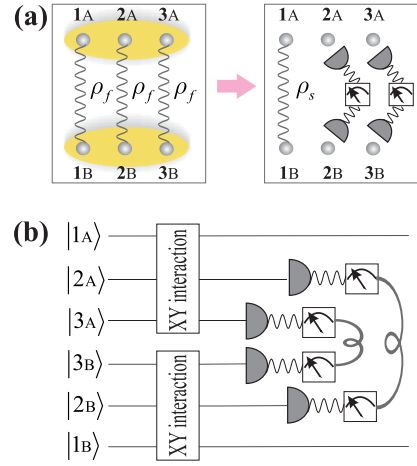


FIG. 2. (Color online) (a) Sequence of steps for the proposed purification scheme using a single elementary block containing three low-fidelity entangled pairs. See text for description. (b) Quantum circuit that corresponds to the interaction depicted above by grey ellipses.

2_B . In this case, the (unmeasured) qubit pair $1_A - 1_B$ is described by the Bell-diagonal density operator ρ_s that implies the fidelity (we drop super- and subscripts AB)

$$\mathbf{F}(\rho_s) \equiv \text{Tr} [\Phi^+ \rho_s] = \frac{1 - 2f + 10f^2}{5 - 4f + 8f^2}, \quad (3)$$

such that $\mathbf{F}(\rho_s) > \mathbf{F}(\rho_f)$ for any $f > 0.5$. The entanglement purification is unsuccessful if the mentioned outcome of projections reads $\{0, 1\}$ or $\{1, 0\}$ and the qubit pair $1_A - 1_B$ must be discarded. Successfully purified pairs, in contrast, are collected from all blocks in order to carry out the next purification round as illustrated in the lower part of Fig. 1(a). At every purification round, high-fidelity entangled pairs are distilled from a larger set of low-fidelity pairs and the described procedure can be straightforwardly extended to more subsequent purification rounds once a sufficient amount of elementary blocks is provided at the input.

Obviously, any practical purification scheme has to be resource-efficient and involve experimentally feasible qubit operations. The above purification protocol, however, involves cumbersome CNOT gates which pose a serious challenge for most physical realizations of qubits, involving complicated pulse sequences along with superfluous qubit operations [10, 30–34]. In the current work, we present a more practical bipartite purification scheme that exploits the *natural dynamics* of spin chains and can be straightforwardly realized in the framework of cavity QED. In contrast to conventional purification protocols (such as described above), in our purification scheme, (i) each elementary block contains three qubit pairs as displayed in Fig. 2(a), (ii) single-qubit U_{\pm} rotations together with CNOT gates are replaced by Heisenberg XY interactions as shown in Fig. 2(b), and (iii) two qubit pairs

from each elementary block are projectively measured out after the interaction [see the right part of Fig. 2(a)]. Entanglement purification is successful if the combined outcome of the projections coincides with a predefined outcome that is determined by the Heisenberg XY model (see Section II C).

Although we increase the number of qubit pairs inside each elementary block in our scheme, in every purification gate we avoid the direct use of CNOT gates together with single-qubit rotations and hence the need for complicated pulse sequences and extra qubit operations. The interaction based on the Heisenberg XY model, moreover, describes the natural dynamics of spin chains that is characteristic for many physical realizations of qubits. It can be deterministically obtained in the framework of cavity QED by using short chains of atoms coupled to the same cavity mode of a high-finesse optical resonator (see Refs. [32, 35] for the simplest case with two atoms).

In the present work, we develop an experimentally feasible purification scheme which exploits a cavity-mediated interaction between atoms that produces a Heisenberg XY type evolution. This results in a more resource- and time-efficient protocol if compared with conventional approaches. Following the recent developments in cavity QED, moreover, we briefly point to and discuss a few practical issues related with the implementation of our purification scheme and the main limitations which may arise on the experimental side. By combining our purification scheme with entanglement distribution and swapping protocols, a reasonably practical implementation of resource- and time-efficient quantum repeaters for long-distance quantum communication using chains of atoms and optical resonators may be possible.

The paper is organized as follows. In the next section, we first outline our purification scheme. We analyze the atomic evolution that is mediated by the cavity field in subsection II.A. In subsection II.B, we derive the effective Hamiltonian that governs this evolution and we identify it with the Heisenberg XY model. In subsection II.C, we apply the dynamics of the derived Hamiltonian to our purification scheme and determine the main properties which are relevant for our scheme. In subsections II.D - II.E, we discuss several issues which follow from the analysis performed in the preceding subsections and which are crucial for our purification scheme. We discuss one issue related to the implementation of our purification scheme in subsection II.F, while a short summary and outlook are given in section III.

II. PURIFICATION PROTOCOL WITHOUT CNOT GATES

The main physical resources of our purification scheme are: (i) chains of atoms, (ii) high-finesse optical cavities, and (iii) detectors for projective measurement of atomic states. In Fig. 3(a) we show a scheme of the proposed quantum repeater segment including two neighbor-

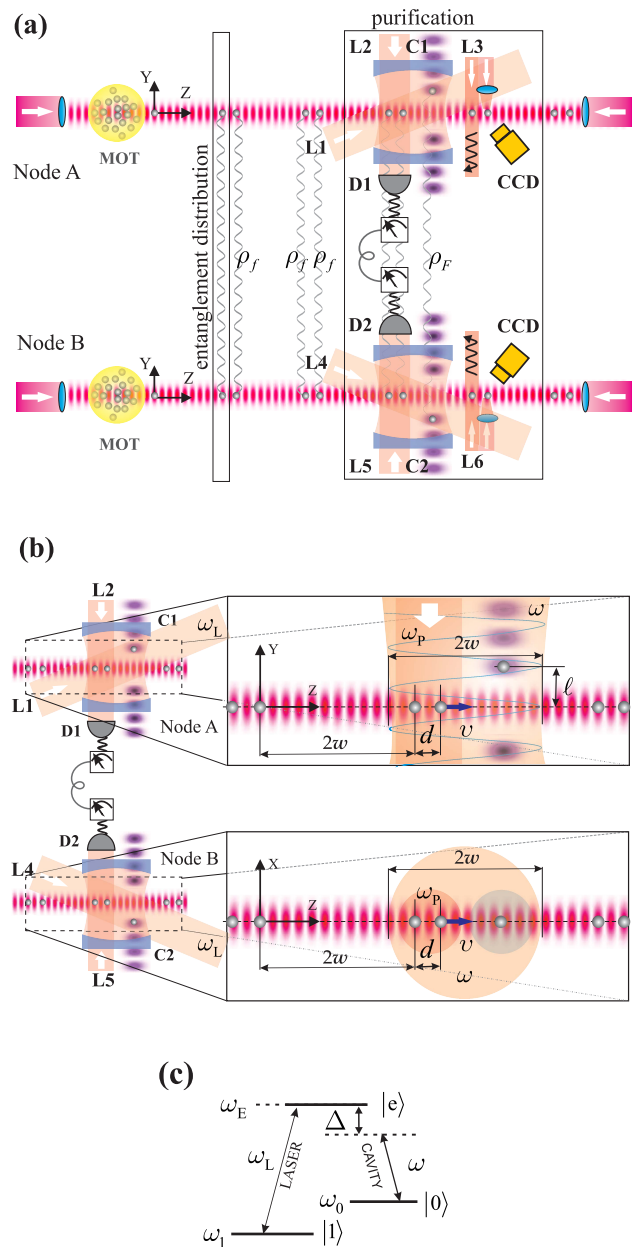


FIG. 3. (Color online) (a) Scheme of an experimental setup that realizes the proposed purification scheme and is incorporated into a quantum repeater segment with two neighboring nodes. See text for description of components. (b) Detailed view of the purification block that is indicated by a rectangle in the above experimental setup. In the upper and lower parts of this figure a magnification of side ($y-z$ plane) and top ($x-z$ plane) views are shown, respectively. See text for description. (c) Structure of three-level atom in the Λ -type configuration.

ing nodes (A and B) and combining entanglement purification and distribution protocols in a single experimental setup. In this setup, each repeater node consists of one optical cavity C_1 (C_2) acting along the y -axis, a laser

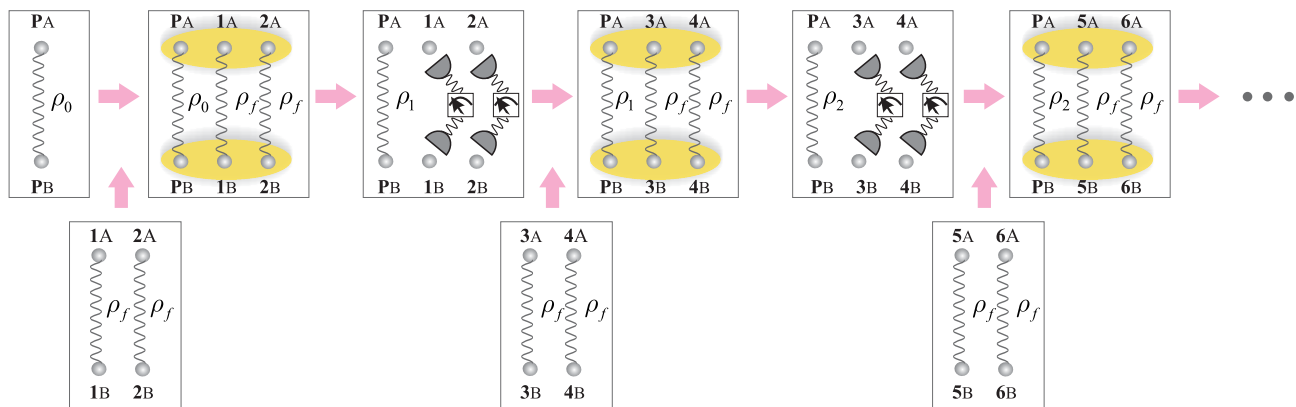


FIG. 4. (Color online) Sequence of steps for the modified entanglement purification scheme that fits the experimental setup from Fig. 3 and which utilizes one single elementary block. This block contains three entangled qubit pairs: (i) one permanent qubit pair that encodes the distilled qubits and (ii) two temporary qubit pairs which are employed to increase the entanglement fidelity of the permanent pair. See text for detailed description.

beam L_1 (L_4), a chain of atoms transported by means of an optical lattice along the along the z -axis, one stationary atom trapped inside the cavity with the help of a vertical lattice, laser beams L_2 (L_5) and L_3 (L_6) which act along the y -axis, a magneto-optical trap (MOT), a detector D_1 (D_2) connected to the neighboring node through a classical communication channel, and a CCD camera. First we shall connect the purification scheme introduced in the previous section with the experimental setup from Fig. 3(a) to clarify the role of each element.

Obviously, the sequence of steps in Fig. 1 with an elementary block displayed in Fig. 2 cannot be directly applied to our experimental setup since it would require one individual cavity for each elementary block and, therefore, an unreasonable demand of physical resources. Instead, we shall consider a modified sequence that is illustrated in Fig. 4 which perfectly fits into our proposed experimental setup. By this sequence, repeater nodes A and B share only one elementary block in which the qubit pair $P_A - P_B$ is a permanent pair and the other two pairs are introduced in the block temporarily in a successive fashion. Initially, there is only one permanent pair in the block that is characterized by the fidelity $\mathbf{F}(\rho_0) > 1/2$ and supplemented by two extra temporary pairs $1_A - 1_B$ and $2_A - 2_B$, both characterized by the fidelity $\mathbf{F}(\rho_f) > 1/2$. Using these three qubit pairs, the sequence displayed in Fig. 2 can now be applied and in the case of successful purification, the increased fidelity $\mathbf{F}(\rho_1)$ of pair $P_A - P_B$, with $\mathbf{F}(\rho_1) > \mathbf{F}(\rho_0)$, is obtained. After the projected pairs $1_A - 1_B$ and $2_A - 2_B$ are replaced with two fresh entangled pairs $3_A - 3_B$ and $4_A - 4_B$, the purification steps are repeated.

While the permanent qubit pair encodes the distilled entangled qubit pair and stores it for the subsequent purification rounds, temporary qubit pairs are used to increase gradually the fidelity of the permanent pair. Below we shall associate permanent qubits with station-

ary atoms trapped inside cavities C_1 and C_2 and temporary qubits with atoms in the chain, inserted into the horizontal lattices and transported along the z -axis [see Fig. 3(a)]. According to our experimental setup, this identification implies that atoms pass sequentially through the cavity and only two atoms from the chain can couple simultaneously to the same cavity mode. These two atoms together with the stationary (trapped) atom, therefore, provide an atomic triplet in each repeater node as required for our purification scheme.

Right before each atom from node A enters the cavity, it becomes entangled with the respective atom from node B as depicted in Fig. 3(a) by wavy lines, such that each entangled pair is described by Eqs. (1)-(2). This entanglement is generated (non-locally) by means of an entanglement distribution block, indicated in Fig. 3(a) by a rectangle. This entanglement distribution may be realized in various ways [26, 36, 37], where our purification protocol here does not depend on any specific choice for the entanglement distribution. During the transition of an atomic pair through the cavity, the triplet of atoms undergoes a cavity-mediated (Heisenberg XY) evolution in each of the repeater nodes, which shall be referred to below as the (new) purification gate. According to the sequence in Fig. 4, furthermore, the purification sequence is completed once the states of a (conveyed) atomic pair are projectively measured and the outcome of projections is pairwise exchanged between the repeater nodes in order to decide if the purification was successful or not.

In our experimental scheme, the latter projections are performed by means of a laser beam L_3 (L_6) and a CCD camera in each of the repeater nodes as displayed in Fig. 3(a). While the laser beam L_3 (L_6) removes atoms in a given quantum state from the chain without affecting atoms in the other state (so-called push-out technique [38]), the CCD camera is used to detect the presence of remaining atoms via fluorescence imaging and determine,

therefore, the state of each atom that leaves the cavity. Assuming that the purification was successful, the next atomic pair from the chain enters the cavity (in each repeater node) and the next purification round occurs with the same stationary atom (permanent qubit). In the unsuccessful case, however, the stationary atoms should be re-initialized and the entire sequence from Fig. 4 should be re-started.

A. Evolution of atoms due to cavity-mediated interaction

We recall that each repeater node disposes N atomic pairs inserted into an optical lattice such that atoms within one pair are separated by a distance d and the distance between two neighboring pairs is adjusted such that only one atomic pair can be coupled simultaneously to the same cavity mode [see Fig. 3(b)]. The entire chain is conveyed with a constant velocity v along the z -axis such that their position vectors $\vec{r}_i(t) = \{0, 0, z_i^o + vt\}$ cross the cavity at the anti-node ($y = 0$) and where z_i^o denotes the initial position of the i -th atom outside the cavity. Both velocity v and inter-atomic distance d can be controlled experimentally by adjusting the shift in the frequencies of the two counter-propagating laser beams and by selecting a proper wavelength of the optical lattice, respectively [41].

Apart from N atomic pairs, moreover, each repeater node contains one stationary atom trapped inside the cavity by a lattice acting along the y -axis. As displayed in Fig. 3(b), the position vector $\vec{r}_s = \{0, \ell, \ell\}$ of this atom crosses the cavity at the anti-node ($y = \ell$) and is located in the same $y-z$ plane as the atomic chain. Each atom in our setup is a three-level atom in the Λ -type configuration as displayed in Fig. 3(c) encoding a single qubit by means of states $|0\rangle$ and $|1\rangle$. In order to protect the qubit against decoherence caused by the fast-decaying excited state $|e\rangle$, the states $|0\rangle$ and $|1\rangle$ are (typically) understood as stable ground and long-living metastable states or two hyperfine levels of the ground state.

We recall, furthermore, that the purification gate from Fig. 2 is based on the Heisenberg XY interaction that is produced deterministically by coupling two-level atoms to the same mode of a high-finesse resonator in our scheme. Due to the encoding scheme from Fig. 3(c), however, the detuned optical cavity is coupled to the atomic transition $|0\rangle \leftrightarrow |e\rangle$, while the atomic qubit is stored by means of states $|0\rangle$ and $|1\rangle$. In order to couple the atomic qubit to the cavity, therefore, an intermediate excitation coupled to the $|1\rangle \leftrightarrow |e\rangle$ transition is further required in order to transfer coherently the electronic population of atoms from the qubit-storage states $\{|0\rangle, |1\rangle\}$ to the cavity-active states $\{|0\rangle, |e\rangle\}$. For this reason, the laser beam L_1 (L_4) is introduced in our experimental setup and coupled resonantly to the $|1\rangle \leftrightarrow |e\rangle$ transition.

Right after the atomic pair is loaded into the cavity, this laser beam is switched on for a short time period that

is equivalent to a $\pi/2$ Rabi pulse. Under the action of this pulse, the laser field couples simultaneously to the atomic triplet (atomic pair from the chain and stationary atom) and transfers coherently the electronic population of each atom from the qubit-storage to cavity-active states. This coherent transfer, in turn, couples the atomic triplet to the cavity and activates the cavity-mediated evolution within this atomic triplet. In the same fashion, one additional laser pulse applied after the operational time that is required for the purification gate, transfers coherently the atomic population from the cavity-active to qubit-storage states backwards and stops the cavity-mediated evolution. By switching appropriately on and off the laser beam L_1 (L_4), therefore, we can precisely control the duration of the cavity-mediated evolution once the atomic pair is conveyed into the the cavity.

Before we turn to the Hamiltonian that governs the evolution of atoms coupled to the same cavity mode, it is important to explain the mechanism of cavity-mediated evolution of an atomic triplet. Let us consider, for instance, three atoms prepared initially in the product state: $|e_1, 0_2, 0_3\rangle$, where the subscripts 1 and 2 correspond to the atomic pair from the chain with position vectors $\vec{r}_1(t)$ and $\vec{r}_2(t)$, respectively, while the subscript 3 corresponds to the stationary atom with position vector $\vec{r}_3 \equiv \vec{r}_s$. In this case, composite atomic states evolve according to the sequences:

$$|e_1, 0_2, 0_3; \bar{0}\rangle \rightarrow |0_1, 0_2, 0_3; \bar{1}\rangle \begin{cases} \nearrow |0_1, e_2, 0_3; \bar{0}\rangle \\ \searrow |0_1, 0_2, e_3; \bar{0}\rangle \end{cases}, \quad (4)$$

if there were initially no photons in the cavity.

The middle part of the above sequence describes the cavity-mediated interaction between the atoms realized by means of a single-photon exchange. In order to avoid the (fast decaying) cavity-excited state $|0_1, 0_2, 0_3; \bar{1}\rangle$ and ensure that the cavity remains (almost) unpopulated during the entire evolution, we require a rather large detuning between the atomic $|0\rangle \leftrightarrow |e_i\rangle$ transition and the resonant frequency of the cavity field

$$|(\omega_E - \omega_0) - \omega| \gg g(\vec{r}_i), \quad i = 1, 2, 3, \quad (5)$$

where ω is the resonant frequency of the cavity field and

$$g(\vec{r}) = g_o \exp[-(z^2 + x^2)/w^2] \quad (6)$$

is the (position-dependent) atom-cavity coupling¹. This position-dependence is caused by the variation of the transversal cavity field along atomic trajectories, where

¹ Gaussian beam that is formed inside a cavity depends on the y -coordinate by means of width of Gaussian beam, radius of curvature, and Guoy phase [55]. To a good approximation, however, we can neglect this dependence if the distance between two cavity anti-nodes (to which atomic pair and stationary atom are coupled) is relatively small.

g_o denotes the vacuum Rabi frequency and w is the cavity field waist as seen in Fig. 3(b).

With help of condition (5), the sequence (4) reduces to the effective sequence

$$|e_1, 0_2, 0_3\rangle \begin{cases} \nearrow |0_1, e_2, 0_3\rangle \\ \searrow |0_1, 0_2, e_3\rangle \end{cases}, \quad (7)$$

where the (fast decaying) cavity-excited state has been omitted. By composing effective sequences for the remaining (three-qubit) product states, we conclude that this evolution preserves the number of excitations in the system and all composite atomic states can be divided in four decoupled (non-overlapping) sub-spaces: (i) $|0_1, 0_2, 0_3\rangle$, (ii) $|e_1, 0_2, 0_3\rangle$, $|0_1, e_2, 0_3\rangle$, $|0_1, 0_2, e_3\rangle$, (iii) $|e_1, e_2, 0_3\rangle$, $|0_1, e_2, e_3\rangle$, $|e_1, 0_2, e_3\rangle$, and (iv) $|e_1, e_2, e_3\rangle$. This conclusion implies, moreover, that the states from groups (i) and (iv) remain trapped with regard to the cavity-mediated evolution.

B. Effective Hamiltonian associated with the cavity-mediated evolution

While the effective sequence (7) displays the cavity-mediated evolution of three atoms, we still have to analyze this evolution quantitatively in order to understand how to control it in practice. For this purpose, we shall adiabatically eliminate the intermediate state which we omitted in the effective sequence and shall derive an effective Hamiltonian that governs the evolution associated with this sequence. For three identical atoms which are coupled simultaneously to the same cavity mode, the evolution of the combined triplet-cavity system is governed by the Jaynes-Cummings Hamiltonian

$$H_{JC}(t) = -\hbar \Delta a^\dagger a - i \hbar \sum_{k=1}^3 g_k(t) \left(a \sigma_k^\dagger - a^\dagger \sigma_k \right). \quad (8)$$

In this Hamiltonian, a and a^\dagger denote the annihilation and creation operators for a cavity photon that acts upon the Fock states $|\bar{n}\rangle$, while $\sigma_i = |0\rangle_i \langle e|$ and $\sigma_i^\dagger = |e\rangle_i \langle 0|$ are the atomic lowering and raising operators, respectively. Moreover, $\Delta = (\omega_E - \omega_0) - \omega$ refers to the detuning as displayed in Fig. 3(c) and the atom-cavity couplings

$$g_i(t) \equiv g(\vec{r}_i) = g_o \exp \left[-(z_i^o + vt)^2/w^2 \right], \quad i = 1, 2, \quad (9)$$

$$g_3(t) \equiv g(\vec{r}_s) = g_o \exp \left[-\ell^2/w^2 \right],$$

have been introduced, such that $|z_1^o - z_2^o| = d$. The time evolution governed by this Hamiltonian, furthermore, is described by the Schrödinger equation

$$i \hbar \frac{d|\psi(t)\rangle}{dt} = H_{JC}(t) |\psi(t)\rangle. \quad (10)$$

As we explained above, all composite atomic states are divided in four decoupled sub-spaces such that evolution

(10) preserves the number of excitations in the system. Therefore, we can consider one particular ansatz for the wave-function

$$|\psi(t)\rangle = c_0(t) |0_1, 0_2, 0_3; \bar{1}\rangle + c_1(t) |e_1, 0_2, 0_3; \bar{0}\rangle + c_2(t) |0_1, e_2, 0_3; \bar{0}\rangle + c_3(t) |0_1, 0_2, e_3; \bar{0}\rangle, \quad (11)$$

that is based on sequence (4). In the above ansatz, we assume that $c_0(t), \dots, c_3(t)$ are the complex and normalized amplitudes, such that $c_0(0) = 0$. Using ansatz (11), the Schrödinger equation (10) gives rise to the closed system of equations

$$i \dot{c}_0(t) = -\Delta c_0(t) + i \sum_{k=1}^3 g_k(t) c_k(t), \quad (12a)$$

$$\dot{c}_i(t) = -g_i(t) c_0(t), \quad i = 1, 2, 3, \quad (12b)$$

which describes the evolution of the coupled atoms-cavity system that is governed by the Hamiltonian (8), and where dot denotes the time derivative.

According to the sequence (7), the state $|0_1, 0_2, 0_3; \bar{1}\rangle$, remains (almost) unpopulated once the atom-cavity detuning is chosen properly [see Eq. (5)]. In order to separate the evolution of unpopulated states from Eqs. (12), we apply the adiabatic elimination procedure which assumes an adiabatic behavior of the amplitudes $c_0(t)$ and, hence, to a good approximation vanishing of its time derivatives (see, for instance, Ref. [42]). We exploit this derivative $\dot{c}_0(t) \cong 0$ and obtain with help of Eq. (12a) an equation for $c_0(t)$ which we insert into Eq. (12b). The remaining three effective equations,

$$i \dot{c}_k(t) = \sum_{j=1}^3 \frac{g_k(t) g_j(t)}{\Delta} c_j(t), \quad (13)$$

describe only the amplitudes $c_1(t)$, $c_2(t)$, $c_3(t)$ which correspond to the states $|e_1, 0_2, 0_3\rangle$, $|0_1, e_2, 0_3\rangle$, $|0_1, 0_2, e_3\rangle$, respectively.

Above equations which we derived from Eqs. (12) by using the adiabatic elimination procedure, in turn, can be derived directly from the Schrödinger equation

$$i \hbar \frac{d|\phi(t)\rangle}{dt} = H(t) |\phi(t)\rangle, \quad (14)$$

$$|\phi(t)\rangle = c_1(t) |e_1, 0_2, 0_3\rangle + c_2(t) |0_1, e_2, 0_3\rangle + c_3(t) |0_1, 0_2, e_3\rangle,$$

associated with the effective Hamiltonian

$$H(t) = \hbar \sum_{k=1}^3 \frac{g_k(t)^2}{\Delta} |e\rangle_k \langle e| + \tilde{H}(t), \quad (15)$$

$$\tilde{H}(t) = \hbar \sum_{\substack{i,j=1 \\ (i \neq j)}}^3 \frac{g_i(t) g_j(t)}{\Delta} \left(\sigma_i^\dagger \sigma_j + \sigma_j^\dagger \sigma_i \right), \quad (16)$$

describing the evolution due to the effective sequence (7), and where $\tilde{H}(t)$ is the dipole-dipole interaction that describes the cavity-mediated energy exchange between the

atoms. As a summary, we have shown that the evolution of an atomic triplet coupled to the detuned cavity field is reduced to the evolution of atoms which interact via single-photon exchange in such a manner that the cavity-excited state remains (almost) unpopulated.

The Hamiltonian (15) is complicated to handle analytically since it contains time-dependent (atom-cavity) couplings (9). In order to simplify our further analysis and approximate reasonably well the evolution given by the Hamiltonian (15), we calculate first the mean values of atom-cavity couplings and consider these instead of the time-dependent couplings in the above Hamiltonian. In order to proceed, we assume that the atomic triplet interacts with the cavity field during the entire transition time, in which the atomic pair is conveyed through the (waist region w of the) cavity field. We note, moreover, that the first term in the Hamiltonian (15) doesn't contribute to the cavity-mediated energy exchange between the atoms that is essential for our protocol. Therefore, we ignore this term while calculating the mean values of atom-cavity couplings and we integrate the Eq. (14) with $H(t)$ being replaced by $\tilde{H}(t)$

$$i\hbar \frac{d|\phi(t)\rangle}{dt} = \tilde{H}(t) |\phi(t)\rangle. \quad (17)$$

To a good approximation, the commutator $[\tilde{H}(t_1), \tilde{H}(t_2)]$ vanishes for all t_1 and t_2 because of a rather large detuning Δ in the denominator of Eq. (16) as compared to the quadratic atom-cavity coupling in the nominator [see Eq. (5)]. In a high-finesse cavity, moreover, the Gaussian envelope (9) describes quite well the strength of the atom-cavity coupling and, therefore, we can safely integrate Eq. (17) from $t \rightarrow -\infty$ to $t \rightarrow +\infty$

$$U(\infty) = \exp \left[-\frac{i}{\hbar} \int_{-\infty}^{\infty} \tilde{H}(t) dt \right] = \exp \left[-\frac{i}{\hbar} H_{\infty} t' \right], \quad (18)$$

where $t' \equiv \sqrt{\pi} w/v$ is the effective interaction time, and the asymptotic Hamiltonian H_{∞} is defined in the form

$$H_{\infty} = \frac{\hbar g_o^2 e^{-\ell^2/w^2}}{\Delta} \sum_{\substack{i,j=1 \\ (i \neq j)}}^3 C_{ij} \left(\sigma_i^{\dagger} \sigma_j + \sigma_j^{\dagger} \sigma_i \right), \quad (19)$$

with the coupling-terms $C_{13} = C_{31} = C_{23} = C_{32} = 1$,

$$\text{and} \quad C_{12} = C_{21} = \frac{1}{\sqrt{2}} \exp \left[\frac{2\ell^2 - d^2}{2w^2} \right]. \quad (20)$$

By inserting the mean atom-cavity couplings from the asymptotic Hamiltonian (19) into the effective Hamiltonian (15), we obtain the mean Hamiltonian in the form

$$H_M = \frac{\hbar g^2}{\Delta} \left[\sum_{k=1}^3 |e\rangle_k \langle e| + \sum_{\substack{i,j=1 \\ (i \neq j)}}^3 \left(\sigma_i^{\dagger} \sigma_j + \sigma_j^{\dagger} \sigma_i \right) \right], \quad (21)$$

where $g \equiv g_o e^{-\ell^2/2w^2}$ is the mean atom-cavity coupling, and where we assumed that distances d and ℓ are adjusted

such that $C_{12} = C_{21} = 1$. In an appropriate interaction picture, furthermore, the mean Hamiltonian (21) can be expressed in the simplified form

$$\begin{aligned} H_I &= \frac{\hbar g^2}{\Delta} \sum_{\substack{i,j=1 \\ (i \neq j)}}^3 \left(\sigma_i^{\dagger} \sigma_j + \sigma_j^{\dagger} \sigma_i \right) \\ &= \frac{\hbar J}{2} \sum_{i=1}^3 \left(\sigma_i^x \sigma_{i+1}^x + \sigma_i^y \sigma_{i+1}^y \right), \end{aligned} \quad (22)$$

which coincides with the isotropic Heisenberg XY interaction Hamiltonian with periodic boundary conditions, i.e., $\sigma_4^x = \sigma_1^x$ and $\sigma_4^y = \sigma_1^y$ [43], and where $J \equiv g^2/\Delta$ is the coupling between three spins. This coupling, moreover, can be positive or negative depending on the sign of the atom-cavity detuning Δ [see Fig. 3(c)].

To summarize this section, we calculated first the effective Hamiltonian (15) starting from Eqs. (10), (11) with help of the adiabatic elimination procedure. Secondly, we obtained the mean values of atom-cavity couplings from the asymptotic Hamiltonian (19) and derived the mean Hamiltonian (22). We stress, moreover, that the ansatz (11) is based on those composite atomic states from group (ii) which involve one single excitation. It can be shown, however, that Hamiltonian (22) preserves the number of excitations in the system and it describes correctly the atomic evolution that is based on the composite atomic states from groups (i), (iii), and (iv).

C. Dynamics of Heisenberg XY model and purification protocol

In the previous subsection, we identified the cavity-mediated evolution of an atomic triplet with the evolution of three spins which interact by means of the isotropic Heisenberg XY Hamiltonian with periodic boundary conditions. In the framework of cavity QED, therefore, the purification gate that is required for our scheme can be deterministically realized by coupling an atomic triplet to the same (detuned) cavity mode for a predefined time period. In this section, we shall analyze the evolution governed by the Heisenberg XY Hamiltonian (22) and determine its properties along with necessary operational times.

Earlier we explained that right before each atomic pair from node A enters the cavity, it becomes entangled pairwise with another atomic pair from node B as depicted in Fig. 3(a) by wavy lines. We denote two conveyed pairs of atoms in the nodes A and B with labels 1, 2 and 4, 5, respectively, while the stationary atoms are labeled by 3 and 6, respectively. By this notation, the conveyed atomic pairs are described by the density operators $\rho_f^{1,4}$ and $\rho_f^{2,5}$, while the pair of stationary atoms is described by the density operator $\rho_{f'}^{3,6}$. Since each purification round should lead to a gradual growth of entanglement fidelity (for the stationary atoms), we distinguish

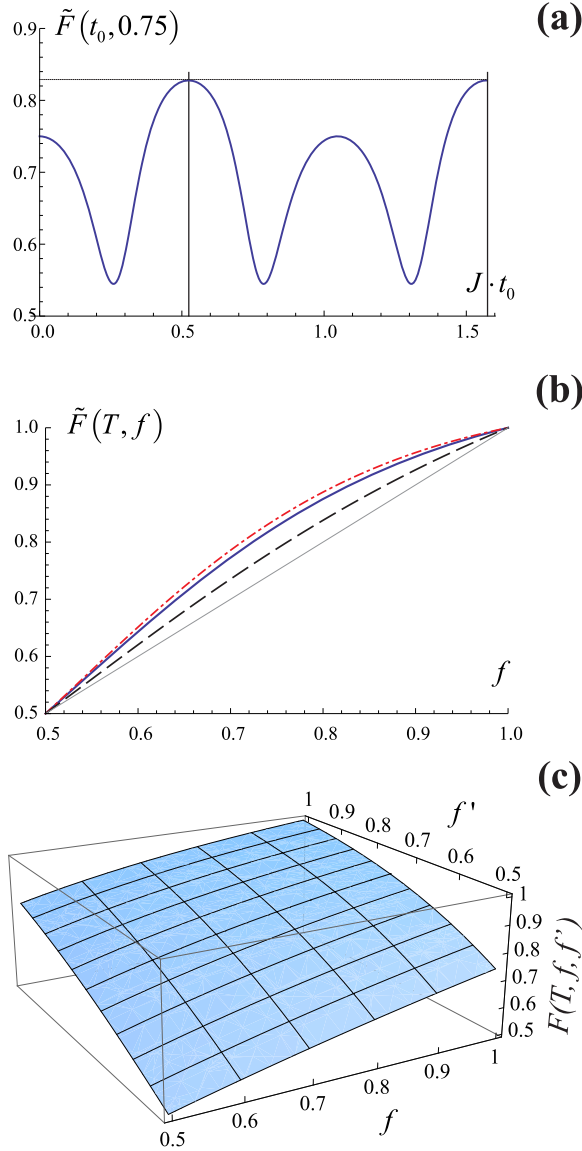


FIG. 5. (Color online) (a) Fidelity $\tilde{F}(t, 0.75)$ as a function of operational time t_0 with fixed input fidelity $f = 0.75$. (b) Fidelity $\tilde{F}(T, f)$ (solid curve) as a function of input fidelity f with fixed operational time given by Eq. (32). Behavior of Eq. (3) (dashed curve) obtained in the conventional (CNOT-based) purification protocol after one purification round. Fidelity (dot-dashed curve) obtained after two (successful) purification steps using the scheme C from Ref. [46] (see discussions in the text). (c) Fidelity $F(T, f, f')$ as a function of input fidelities f and f' associated with the conveyed atomic pairs and the stationary atomic pair, respectively, with the operational time T given by Eq. (32).

the initial fidelities f of conveyed atomic pairs from the fidelity f' of stationary atoms.

The evolution associated with the Hamiltonian (22),

$$U_I(t) = e^{-\frac{i}{\hbar} H_I t} = \sum_{k=1}^8 e^{-\frac{i}{\hbar} E_k t} |k\rangle\langle k|, \quad (23)$$

is completely determined by the energies E_k and vectors $|k\rangle$ given in the cavity-active basis $\{|0\rangle, |e\rangle\}$, which satisfy the equality $H_I |k\rangle = E_k |k\rangle$ with orthogonality and completeness relations $\langle k|k'\rangle = \delta_{kk'}$ and $\sum |k\rangle\langle k| = I$, respectively. This eigenvalue problem has been exactly solved with help of the Jordan-Wigner transformation [44] and its respective solutions have been presented in the literature (see, for instance, Ref. [45]). Since the evolution operator (23) acts on the states of one atomic triplet that is pairwise entangled with another atomic triplet (in the neighboring node), we have to consider the composite evolution operator

$$U(t) = \sum_{k, k'=1}^8 e^{-\frac{i}{\hbar} (E_k + E_{k'}) t} |k_A \otimes k'_B\rangle\langle k_A \otimes k'_B|. \quad (24)$$

According to this evolution operator, the state of both atomic triplets in nodes A and B is described by the six-qubit density operator

$$\rho^{1-6}(t, f, f') = U(t) \left(\rho_f^{1,4} \otimes \rho_{f'}^{2,5} \otimes \rho_{f'}^{3,6} \right) U^\dagger(t), \quad (25)$$

where the states of each atomic triplet have been coherently mapped from the qubit-storage basis $\{|0\rangle, |1\rangle\}$ to the cavity-active basis $\{|0\rangle, |e\rangle\}$ by means of the laser beam L_1 (L_4).

Recall that in order to finalize one purification round, we map back the states of both atomic triplets from the cavity-active basis $\{|0\rangle, |e\rangle\}$ to the qubit-storage basis $\{|0\rangle, |1\rangle\}$ and project both (conveyed) atomic pairs once they leave their cavities. This implies that after an evolution time $t = t_0$, during which the atoms evolved due to cavity-mediated interaction and that is followed by the mapping $\{|0\rangle, |e\rangle\} \rightarrow \{|0\rangle, |1\rangle\}$, the state of both atomic triplets in nodes A and B is described by the density operator

$$\tilde{\rho}^{1-6}(t_0, f, f') = \sum_{i,j=1}^{64} \rho_{ij}^{1-6}(t_0, f, f') |\mathbf{V}_i\rangle\langle \mathbf{V}_j|, \quad (26)$$

where the composite six-qubit vectors $|\mathbf{V}_i\rangle$ are given in the computational (qubit-storage) basis $\{|0\rangle, |1\rangle\}$ and satisfy the orthogonality and completeness relations $\langle \mathbf{V}_i | \mathbf{V}_j \rangle = \delta_{ij}$ and $\sum |\mathbf{V}_i\rangle\langle \mathbf{V}_i| = I$, respectively. Once both (conveyed) atomic pairs leave their cavities, the projective measurements of their states is performed and the whole sequence of steps leads to the density operator and the probability of success,

$$\rho^{3,6}(t_0, f, f') = \frac{\sum_{\alpha,\beta} \rho_{\alpha\beta}^{1-6}(t_0, f, f')}{P_{\text{succ}}(t_0, f, f')} |\tilde{\mathbf{V}}_\alpha\rangle\langle \tilde{\mathbf{V}}_\beta|, \quad (27)$$

$$P_{\text{succ}}(t_0, f, f') = \text{Tr} \left[\sum_{\alpha,\beta} \rho_{\alpha\beta}^{1-6}(t_0, f, f') |\tilde{\mathbf{V}}_\alpha\rangle\langle \tilde{\mathbf{V}}_\beta| \right],$$

that describes only the state of stationary atoms, and where the Greek indices run over four values i_1, i_2, i_3, i_4 or j_1, j_2, j_3, j_4 such that $|\tilde{\mathbf{V}}_\alpha\rangle \equiv \langle 0_1, 1_2, 0_4, 1_5 | \mathbf{V}_\alpha \rangle \neq 0$ or $|\tilde{\mathbf{V}}_\alpha\rangle \equiv \langle 1_1, 0_2, 1_4, 0_5 | \mathbf{V}_\alpha \rangle \neq 0$, respectively. As we shall see below, one of the two outcomes (of projective measurements),

$$\{0_1, 1_2, 0_4, 1_5\} \quad \text{or} \quad \{1_1, 0_2, 1_4, 0_5\}, \quad (28)$$

is the necessary condition to complete successfully one purification round and increase the entanglement fidelity associated with the stationary atoms.

According to the six-qubit density operator (25), we have routinely computed the matrix elements

$$\tilde{F}(t_0, f) = \frac{f - 38f^2 - 8 + 8(1 - 5f + 4f^2) \cos(6Jt_0) - 12f(4f - 1) \cos(12Jt_0)}{34f - 32f^2 - 47 + 16(1 - 5f + 4f^2) \cos(6Jt_0) - 4(2f + 8f^2 - 1) \cos(12Jt_0)}, \quad (30)$$

$$\tilde{P}_{\text{succ}}(t_0, f) = (1 + 2f) [47 - 34f + 32f^2 - 16(1 - 5f + 4f^2) \cos(6Jt_0) + 4(2f + 8f^2 - 1) \cos(12Jt_0)] / 972. \quad (31)$$

In Fig. 5(a), we display $\tilde{F}(t_0, f)$ as a function of t_0 for the input fidelity $f = 0.75$. It is clearly seen that after the time interval $t_0 = T$ that satisfies ($n = 0, 1, 2, \dots$),

$$JT = \frac{\pi}{3} \left(n + \frac{1}{2} \right), \quad (32)$$

this fidelity reaches its maximum value $\cong 0.827$. This equality, therefore, sets the operational time that is required for execution of the purification gate and which makes the output fidelity $\tilde{F}(T, f)$ increase with regard to its input value f . Corresponding to this operational time, furthermore, the fidelities $F(T, f, f')$ and $\tilde{F}(T, f)$ along with the success probabilities $P_{\text{succ}}(T, f, f')$ and $\tilde{P}_{\text{succ}}(T, f)$ take the following simplified form,

$$F(T, f, f') = \frac{f'(12f + 236f^2 - 5) - 16(f - 1)}{59 + (12 - 64f')f - 4(5 - 64f')f^2},$$

$$\tilde{F}(T, f) = \frac{16 - 53f + 118f^2}{59 - 106f + 128f^2}, \quad (33)$$

$$P_{\text{succ}}(T, f, f') = \frac{59 + (12 - 64f')f + 4(-5 + 64f')f^2}{972},$$

$$\tilde{P}_{\text{succ}}(T, f) = (59 + 12f - 84f^2 + 256f^3) / 972. \quad (34)$$

The first two expressions describe quantitatively how the input fidelity of stationary atoms is modified due to one single (and successful) round of our purification scheme. In Fig. 5(b), we compare the fidelity $\tilde{F}(T, f)$ (solid curve) with the fidelity given by Eq. (3) (dashed curve) that is obtained due to a single successful purification round in the conventional (CNOT-based) protocol. This comparison shows that the increase of fidelity in our scheme is almost twice as large as for the conventional protocol. This nice result, however, originates merely from the fact that our scheme requires one extra qubit

$\rho_{\alpha\beta}^{1-6}(t_0, f, f')$ which, however, are rather bulky to be displayed here. The first relevant result we obtain with help of these matrix elements is that the density operator (27) preserves the diagonal form in the Bell basis,

$$\rho^{3,6}(t_0, f, f') = F \Phi_{36}^+ + \frac{1-F}{3} (\Phi_{36}^- + \Psi_{36}^+ + \Psi_{36}^-). \quad (29)$$

Unlike the conventional purification protocol, therefore, the purified state (29) is a Werner state that is completely characterized by the fidelity $\mathbf{F}(\rho^{3,6}) = F(t_0, f, f')$, where the functions $\tilde{F}(t_0, f) \equiv F(t_0, f, f)$ and $\tilde{P}_{\text{succ}}(t_0, f) \equiv P_{\text{succ}}(t_0, f, f)$ have the form

pair for a single purification round. Being projectively measured right after the first pair, this extra pair leads to a stronger entanglement distillation of the stationary atoms in the case of successful purification.

In order to motivate the latter conclusion, recall that we considered the purification sequence displayed in Fig. 4 that fits perfectly our experimental setup from Fig. 3. In fact, this sequence is similar to scheme C of W. Dür and co-authors, as presented in Ref. [46], using CNOT gates and freshly prepared entangled pairs for every single purification step (so-called *entanglement pumping*). In this (CNOT-based) scheme, therefore, the number of atomic pairs required for two purification rounds (one permanent pair and two successive temporary pairs) coincides with the number of atomic pairs as required for one single purifications round in our scheme. For this equal amount of atomic resources, we plotted in Fig. 5(b) the fidelity (dot-dashed curve) obtained after two (successful) purification rounds using the scheme C by W. Dür and co-authors. It is clearly seen that this fidelity deviates only slightly from the fidelity (solid curve) obtained after one single purification round in our scheme.

Apparently, our purification scheme is useful only if each round leads to a gradual growth of entanglement fidelity (of yjr stationary atoms) with regard to the respective fidelity obtained in the previous round, i.e.,

$$f' < F_1(T, f, f') < F_2(T, f, F_1) < \dots < F_n(T, f, F_{n-1}). \quad (35)$$

In Fig. 5(c), we displayed the output fidelity $F(T, f, f')$ obtained for one single and successful purification round. This fidelity exhibits growth for (one and the same) input fidelity f of the conveyed atomic pairs and (growing) fidelity $f' = F_{n-1}(T, f, F_{n-2})$ of the stationary atomic pair, which was obtained in the previous purification

round. The behavior of output fidelity $F_n(T, f, F_{n-1})$ that is obtained in the n -th purification round, therefore, is in agreement with the sequence (35) and ensures that each successful round leads to a gradual growth of fidelity.

D. Remarks on the entanglement distribution between stationary atomic qubits

Recall that right before each atomic pair from node A enters the cavity, it becomes entangled (pairwise) with another atomic pair from node B, such that the conveyed atomic pairs are described by the density operators $\rho_f^{1,4}$ and $\rho_f^{2,5}$. We assumed, moreover, that the pair of stationary atoms is initially described by the density operator $\rho_{f'}^{3,6}$, however, without explaining how this entangled state is initially created.

In this section, we suggest that there is no need to introduce an additional entanglement distribution device in our experimental setup in order to entangle stationary atoms prior to the purification rounds. Instead, we prepare initially two atoms in the product state $\rho_0^{3,6} = |0_3, 0_6\rangle\langle 0_3, 0_6|$ and start our purification protocol. It can be shown that the first successful round transforms the above product state into an entangled state described by

$$\begin{aligned} \rho_f^{3,6} = & A(f) \Phi_{3,6}^+ + B(f) (\Psi_{3,6}^+ + \Psi_{3,6}^-) + C(f) \Phi_{3,6}^- \\ & + D(f) (|\phi_{3,6}^+\rangle\langle\phi_{3,6}^-| + |\phi_{3,6}^-\rangle\langle\phi_{3,6}^+|) \end{aligned} \quad (36)$$

being off-diagonal in the Bell basis with $A(f) \cong f > 1/2$, such that $\mathbf{F}(\rho_f^{3,6}) > \mathbf{F}(\rho_0^{3,6})$.

Obviously, the above state is no longer a Werner state like in Eq. (29). We verified, however, that the function $D(f)$, which describes off-diagonal contributions, becomes negligibly small after a few successful rounds. Therefore, we succeed to entangle remotely two stationary atoms by means of local (in each repeater node) interactions, such that the input fidelity f of the conveyed atomic pairs is mapped (almost) completely to the output fidelity of the stationary atomic pair. The output fidelity $A(f) \cong f$, plays the role of the input fidelity f' for the next purification round and leads to a gradual growth of entanglement fidelity in agreement with the sequence (35). We have verified, moreover, that the output fidelities due to the initial state (36) coincide (almost) with the output fidelities $F_n(T, f, F_{n-1})$ due to the state (29). The price we pay for one extra (successful) purification round prior to the main sequence of rounds, therefore, is efficiently compensated by a more moderate demand of physical resources in our purification scheme.

E. Saturation of entanglement purification and optimal number of rounds

Recall that instead of the sequence from Fig. 1, we considered a modified sequence displayed in Fig. 4, simi-

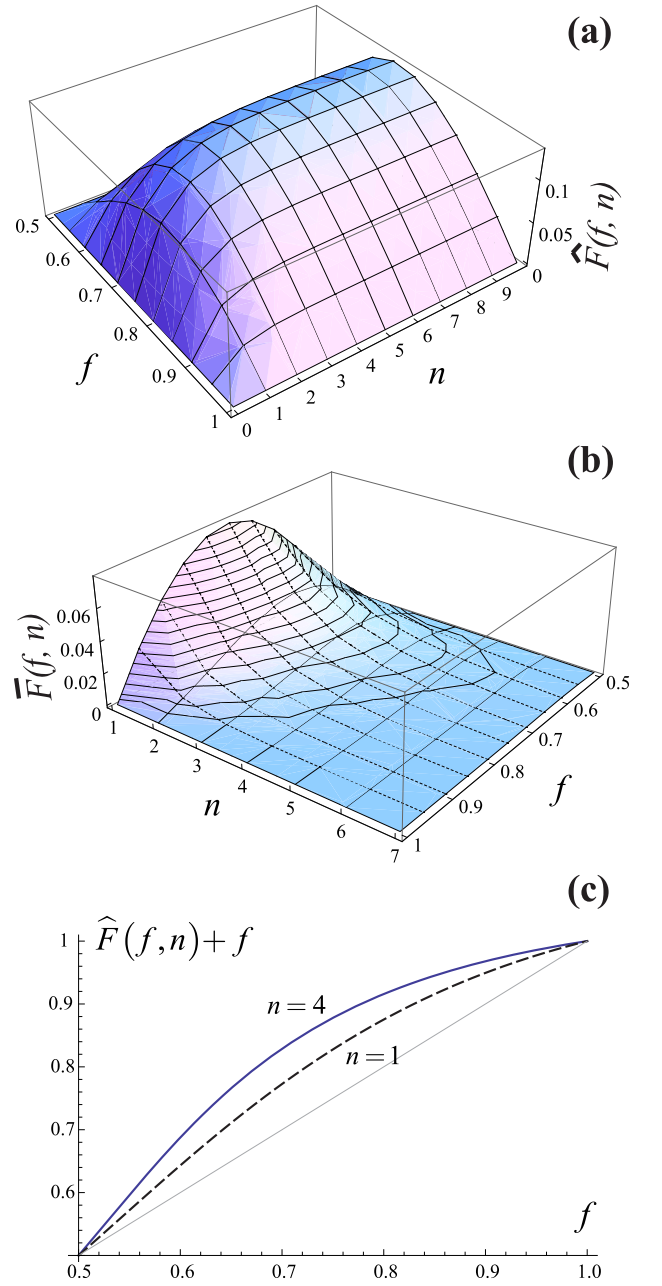


FIG. 6. (Color online) Behavior of (a) $\widehat{F}(f, n)$ and (b) $\bar{F}(f, n)$ as functions of input fidelity f and number n of purification rounds. (c) Final fidelity $\widehat{F}(f, n) + f$ as a function of initial fidelity f with fixed numbers: $n = 4$ (solid curve) and $n = 1$ (dashed curve) of purification rounds.

lar to the scheme C that was proposed and discussed by W. Dür and co-authors with help of CNOT gates [46]. Using this scheme, it has been pointed out that regardless of the number of (successful) purification rounds, the final fidelity is bounded by a fixed point that is smaller than the respective point due to the sequence from Fig. 1.

Similarly, the final fidelity $F_n(T, f, F_{n-1})$ that is obtained at the end of sequence (35) is also bounded by a fixed point in our scheme. In this section, we shall refer to this property as the saturation of entanglement purification and we will calculate the optimal number of (successful) purification rounds that is required to reach closely this fixed point in a resource-efficient way.

While the sequence (35) displays the gradual growth of entanglement fidelity, we still have to analyze this growth quantitatively in order to understand how much the output fidelity increases with each purification round. For this purpose, we shall consider the following sequence,

$$f < F_1(T, f, f) < \dots < F_n(T, f, F_{n-1}) \equiv f + \widehat{F}(f, n). \quad (37)$$

In Fig. 6(a), we show the function $\widehat{F}(f, n)$ that describes the difference between the final fidelity $F_n(T, f, F_{n-1})$ after n (successful) rounds and the initial fidelity f ($n = 0$). It is clearly seen that during the first four successful rounds, this function exhibits a notably fast growth which, however, saturates afterwards and yields a rather minor increase with regard to the fidelity $F_4(T, f, F_3)$.

In order to estimate the relative growth of fidelity that is obtained with each purification round, in Fig. 6(b) we display the function

$$\bar{F}(f, n) = F_n(T, f, F_{n-1}) - F_{n-1}(T, f, F_{n-2}), \quad (38)$$

where $F_0 \equiv f$. This function shows quantitatively how much the output fidelity increases with each purification round in dependence upon both the input fidelity f and the number of rounds n . This time it is clearly seen that the relative growth of fidelity has its maximum for $f = 0.75$ and it mostly vanishes after six successive rounds for all values of f . In dependence upon the input fidelity f , therefore, the surface from Fig. 6(b) enables one to determine the optimal number of (successful) purification rounds n_f that is required to reach closely the fixed point given by $\widehat{F}(f, n_f) + f$.

Corresponding to $n = 4$ purification rounds, for which the final fidelity reaches its saturation level, in Fig. 6(c), we display the fidelity $\widehat{F}(f, n) + f$ for $n = 4$ rounds (solid curve) and the fidelity obtained for $n = 1$ round (dashed curve). By comparing these two curves, we conclude that the increase of final fidelity due to four successive rounds is notably larger if compared to the case of one single purification round. We stress, finally, that W. Dür and co-authors have demonstrated in Ref. [46] that errors and faulty quantum operations may lead to a situation, in which the fixed point in scheme C oversteps the respective fixed point of the conventional protocol based on the sequence from Fig. 1. We expect that a similar behavior may exist in our scheme as well, however, this analysis is beyond the scope of the present paper.

F. Remarks on the implementation of our purification scheme

In our purification scheme, short chains of two atoms (in each repeater node) have to be transported with a constant velocity along the experimental setup and coupled to the cavity field in a well controllable fashion. For this purpose, two basic devices are required to store the atoms and transport them coherently into the cavity, namely, (i) a magneto-optical trap (MOT) that plays the role of an atomic source and (ii) an optical lattice (conveyor belt) that transports atoms into the cavity from the MOT with a certain position and velocity control over the atomic motion. These two tools, combined with a high-finesse optical cavity in the same experimental setup [47–49], enable one to store initiated atoms in the MOT and insert them into the optical lattice for further transportation through the cavity. It has been experimentally demonstrated that an optical lattice preserves the coherence of transported atoms and can be utilized as a holder of a quantum register. Moreover, by encoding the quantum information by means of hyperfine atomic levels, a storage time of the order of seconds has been reported in Refs. [38, 50]. The number-locked insertion technique [51], furthermore, allows to extract atoms from the MOT and insert a predefined pattern of them into an optical lattice with a single-site precision.

III. SUMMARY AND DISCUSSION

In this paper, an experimentally feasible scheme was proposed to purify dynamically entanglement of two atoms which are trapped in two remote optical cavities. Our scheme utilizes chains of low-fidelity entangled atomic pairs which are coupled sequentially to both remote optical cavities. In contrast to conventional purification protocols, we avoid CNOT gates and hence reduce the need for complicated pulse sequences and superfluous qubit operations. Our purification mechanism exploits: (i) cavity-mediated interactions between atoms producing Heisenberg XY evolutions governed by the Hamiltonian (22) and (ii) projective measurements of atomic states. A detailed experimental setup was proposed in Fig. 3 and a complete description of all necessary steps and manipulations was provided. A comprehensive analysis of the fidelity obtained after multiple purification rounds was performed and the optimal number of rounds was determined by means of Fig. 6. Following recent developments in cavity QED, moreover, we briefly pointed to and discussed a few practical issues related to the implementation of our purification scheme, including the main limitations which may arise on the experimental side. We stress that although the proposed purification scheme is experimentally feasible, its complete realization still poses a serious challenge.

Being the most delicate and cumbersome part of a quantum repeater, entanglement purification as proposed

in this paper opens a route towards practical implementations of resource- and time-efficient quantum repeaters for long-distance quantum communication using chains of atoms and optical resonators. In our experimental setup, each atom from node A is assumed to become entangled with another atom from node B right before they enter their respective cavities. This entanglement is generated (non-locally) with help of an entanglement distribution block as indicated in Fig. 3(a) by a rectangle. Since we consider only atoms and optical resonators as the physical resources for our repeater protocol, we suggest for entanglement distribution the scheme proposed in Ref. [26] that allows to entangle non-locally two (three-level) atoms in neighboring repeater nodes.

By this scheme, a coherent-state light pulse interacts with the first coupled atom-cavity system in node A, such that the optical field accumulates a phase conditioned upon the atomic state. After this, the light pulse propagates to repeater node B, where it interacts with the second coupled atom-cavity system and accumulates another phase conditioned upon the state of the atom located in this node. Finally, the phase-rotated coherent state is measured via homodyne detection and an entangled state is non-locally generated through postselection between the atoms belonging to repeater nodes. The controlled phase rotation required for this scheme can be realized by means of a dispersive interaction of a single atom coupled to a high-finesse cavity in each repeater node. A detailed inclusion of this entanglement distribution scheme into our experimental setup is beyond the scope of this paper and will be subject of our next work.

In a recent paper by K. Maruyama and F. Nori [53], a purification mechanism similar to ours and based on the natural dynamics of spin chains has been proposed. In contrast to our approach, however, the purification mechanism of that reference exploits the Heisenberg XYZ

model with open boundary conditions which cannot be straightforwardly realized in the framework of cavity QED. Although the time behavior of our output fidelity $\bar{F}(t, f)$ is different from the respective time behavior found by K. Maruyama and F. Nori (compare Fig. 5(a) with Fig. 3 from Ref. [53]), the Heisenberg XYZ dynamics leads to the same expression (33) for a properly chosen interaction time. Apart from the simplified Hamiltonian utilized in our work, perfectly adapted to the cavity QED framework, the operational time that is required for one purification gate in our scheme is three times faster compared to the Heisenberg XYZ-based dynamics employed by K. Maruyama and F. Nori.

Finally, we would like to mention Ref. [54] by A. Casacino and co-authors in which an entanglement purification protocol based on the Heisenberg XY interaction has also been considered. In contrast to our scheme and the scheme of K. Maruyama and F. Nori, however, in that reference an abstract approach based on the spin dynamics on networks of various topologies has been analyzed. Using this general approach, the authors concluded that the maximum efficiency of entanglement purification is obtained only by means of networks with no isolated nodes. The requirement of no isolated nodes corresponds to the periodic boundary conditions in our approach [see Eq. (22)] and, therefore, we confirmed in our paper the main standpoints of A. Casacino and co-authors from a particular point of view using cavity QED settings.

ACKNOWLEDGMENTS

We thank the DFG for support through the Emmy Noether program. In addition, we thank the BMBF for support through the QuOREP program.

-
- [1] W. K. Wootters and W. H. Zurek, *Nature* **299**, 802 (1982).
 - [2] D. Dieks, *Phys. Lett. A* **92A**, 271 (1982).
 - [3] H.-J. Briegel, W. Dür, J. I. Cirac, and P. Zoller, *Phys. Rev. Lett.* **81**, 5932 (1998).
 - [4] C. H. Bennett, G. Brassard, S. Popescu, B. Schumacher, J. A. Smolin, and W. K. Wootters, *Phys. Rev. Lett.* **76**, 722 (1996).
 - [5] D. Deutsch, A. Ekert, R. Jozsa, C. Macchiavello, S. Popescu, and A. Sanpera, *Phys. Rev. Lett.* **77**, 2818 (1996).
 - [6] M. Zukowski, A. Zeilinger, M. A. Horne, and A. K. Ekert, *Phys. Rev. Lett.* **71**, 4287 (1993).
 - [7] C. H. Bennett, G. Brassard, C. Crépeau, R. Jozsa, A. Peres, and W. K. Wootters, *Phys. Rev. Lett.* **70**, 1895 (1993).
 - [8] N. Gisin, G. Ribordy, W. Tittel, and H. Zbinden, *Rev. Mod. Phys.* **74**, 145 (2002).
 - [9] Z. Zhao, T. Yang, Y.-A. Chen, A.-N. Zhang, and J.-W. Pan, *Phys. Rev. Lett.* **90**, 207901 (2003).
 - [10] R. Reich et al., *Nature* **443**, 838 (2006).
 - [11] T. Yang et al., *Phys. Rev. Lett.* **96**, 110501 (2006).
 - [12] H. de Riedmatten et al., *Phys. Rev. A* **71**, 050302(R) (2005).
 - [13] Z.-S. Yuan, Y.-A. Chen, B. Zhao, S. Chen, J. Schmiedmayer, and J.-W. Pan, *Nature* **454**, 1098 (2008).
 - [14] C.-W. Chou et al., *Science* **316**, 1316 (2007).
 - [15] N. Sangouard, R. Dubessy, and C. Simon, *Phys. Rev. A* **79**, 042340 (2009).
 - [16] B. Zhao, M. Müller, K. Hammerer, and P. Zoller, *Phys. Rev. A* **81**, 052329 (2010).
 - [17] Y. Han, B. He, K. Heshami, C.-Z. Li, and C. Simon, *Phys. Rev. A* **81**, 052311 (2010).
 - [18] J. B. Brask, I. Rigas, E. S. Polzik, U. L. Andersen, and A. S. Sørensen, *Phys. Rev. Lett.* **105**, 160501 (2010).
 - [19] C. Simon, H. de Riedmatten, and M. Afzelius, *Phys. Rev. A* **82**, 010304(R) (2010).
 - [20] A. G. Fowler et al., *Phys. Rev. Lett.* **104**, 180503 (2010).
 - [21] J. B. Brask, L. Jiang, A. V. Gorshkov, V. Vuletic, A. S. Sørensen, and M. D. Lukin, *Phys. Rev. A* **81**,

- 020303(R) (2010).
- [22] N. Sangouard, C. Simon, H. de Riedmatten, and N. Gisin, *Rev. Mod. Phys.* **83**, 33 (2011).
- [23] B.-B. Zhang and Y.-Q. Xu, *Phys. Rev. A* **84**, 014304 (2011).
- [24] P. van Loock, *Laser Photonics Rev.* **5**, 167 (2011).
- [25] N. K. Bernardes, L. Praxmeyer, P. van Loock, *Phys. Rev. A* **83**, 012323 (2011).
- [26] P. van Loock et al., *Phys. Rev. Lett.* **96**, 240501 (2006).
- [27] P. van Loock, N. Lütkenhaus, W. J. Munro, and K. Nemoto, *Phys. Rev. A* **78**, 062319 (2008).
- [28] W. J. Munro, R. Van Meter, S. G. R. Louis, and K. Nemoto, *Phys. Rev. Lett.* **101**, 040502 (2008).
- [29] R. F. Werner, *Phys. Rev. A* **40**, 4277 (1989).
- [30] L. Isenhower et al., *Phys. Rev. Lett.* **104**, 010503 (2010).
- [31] A. Gábris and G. S. Agarwal, *Phys. Rev. A* **71**, 052316 (2005).
- [32] S.-B. Zheng and G.-C. Guo, *Phys. Rev. Lett.* **85**, 2392 (2000).
- [33] T. Tanamoto, K. Maruyama, Y.-X. Liu, X. Hu, and F. Nori, *Phys. Rev. A* **78**, 062313 (2008).
- [34] N. Schuch and J. Siewert, *Phys. Rev. A* **67**, 032301 (2003).
- [35] S. Osnaghi, et al., *Phys. Rev. Lett.* **87**, 037902 (2001).
- [36] J. I. Cirac, P. Zoller, H. J. Kimble, and H. Mabuchi, *Phys. Rev. Lett.*, **78**, 3221 (1997).
- [37] H. J. Kimble, *Nature* **453**, 1023 (2008).
- [38] S. Kuhr et al., *Phys. Rev. Lett.* **91**, 213002 (2003).
- [39] A. D. Boozer, A. Boca, R. Miller, T. E. Northup, and H. J. Kimble, *Phys. Rev. Lett.* **97**, 083602 (2006).
- [40] M. Khudaverdyan, W. Alt, T. Kampschulte, S. Reick, A. Thobe, A. Widera, D. Meschede, *Phys. Rev. Lett.* **103**, 123006 (2009).
- [41] S. Kuhr et al., *Science* **293**, 278 (2001).
- [42] E. Brion, L. H. Pedersen and K. Mølmer, *J. Phys. A: Math. Theor.* **40**, 1033 (2007).
- [43] E. Lieb, T. Schultz, and D. Mattis, *Ann. Phys. (N.Y.)* **16**, 407 (1961).
- [44] P. Jordan and E. Wigner, *Z. Phys.* **47**, 631 (1928).
- [45] X. Wang, *Phys. Rev. A* **64**, 012313 (2001).
- [46] W. Dür, H.-J. Briegel, J. I. Cirac, and P. Zoller, *Phys. Rev. A* **59**, 169 (1999).
- [47] S. Nussmann et al., *Phys. Rev. Lett.* **95**, 173602 (2005).
- [48] K. M. Fortier, S. Y. Kim, M. J. Gibbons, P. Ahmadi, and M. S. Chapman, *Phys. Rev. Lett.* **98**, 233601 (2007).
- [49] M. Khudaverdyan et al., *New J. Phys.* **10**, 073023 (2008).
- [50] D. Schrader, I. Dotsenko, M. Khudaverdyan, Y. Miroshnychenko, A. Rauschenbeutel, and D. Meschede, *Phys. Rev. Lett.* **93**, 150501 (2004).
- [51] M. Karski et al., *New J. of Phys.* **12** 065027 (2010).
- [52] A. S. Sørensen and K. Mølmer, *Phys. Rev. Lett.* **91**, 097905 (2003).
- [53] K. Maruyama and F. Nori, *Phys. Rev. A* **78**, 022312 (2008).
- [54] A. Casaccino, S. Mancini, and S. Severini, *Quant. Inf. Process.* **10**, 107 (2011).
- [55] R. D. Günther, *Modern Optics*, (Wiley, New York, 1990).